

# Effects of Neurotrophin-3 on Intrinsic Neuronal Properties at a Central Auditory Structure

Momoko Takahashi<sup>1</sup>  and Jason Tait Sanchez<sup>1,2,3</sup> 

<sup>1</sup>Roxelyn and Richard Pepper Department of Communication Sciences and Disorders, Northwestern University, Evanston, IL, USA. <sup>2</sup>Department of Neurobiology, Northwestern University, Evanston, IL, USA. <sup>3</sup>The Hugh Knowles Hearing Research Center, Northwestern University, Evanston, IL, USA.

Neuroscience Insights  
Volume 15: 1–13  
© The Author(s) 2020  
Article reuse guidelines:  
sagepub.com/journals-permissions  
DOI: 10.1177/2633105520980442



**ABSTRACT:** Neurotrophins, a class of growth factor proteins that control neuronal proliferation, morphology, and apoptosis, are found ubiquitously throughout the nervous system. One particular neurotrophin (NT-3) and its cognate tyrosine receptor kinase (TrkC) have recently received attention as a possible therapeutic target for synaptopathic sensorineural hearing loss. Additionally, research shows that NT-3-TrkC signaling plays a role in establishing the sensory organization of frequency topology (ie, tonotopic order) in the cochlea of the peripheral inner ear. However, the neurotrophic effects of NT-3 on central auditory properties are unclear. In this study we examined whether NT-3-TrkC signaling affects the intrinsic electrophysiological properties at a first-order central auditory structure in chicken, known as nucleus magnocellularis (NM). Here, the expression pattern of specific neurotrophins is well known and tightly regulated. By using whole-cell patch-clamp electrophysiology, we show that NT-3 application to brainstem slices does not affect intrinsic properties of high-frequency neuronal regions but had robust effects for low-frequency neurons, altering voltage-dependent potassium functions, action potential repolarization kinetics, and passive membrane properties. We suggest that NT-3 may contribute to the precise establishment and organization of tonotopy in the central auditory pathway by playing a specialized role in regulating the development of intrinsic neuronal properties of low-frequency NM neurons.

**KEYWORDS:** Neurotrophin, avian, auditory, brainstem, potassium

**RECEIVED:** June 19, 2020. **ACCEPTED:** November 23, 2020.

**TYPE:** Original Research

**FUNDING:** The author(s) disclosed receipt of the following financial support for the research, authorship, and/or publication of this article: Research supported by the National Institute on Deafness and Other Communication Disorders (NIDCD) R01 DC013841 (JTS) and the Hugh Knowles Hearing Research Center (JTS).

**DECLARATION OF CONFLICTING INTERESTS:** The author(s) declared no potential conflicts of interest with respect to the research, authorship, and/or publication of this article.

**CORRESPONDING AUTHOR:** Jason Tait Sanchez, Roxelyn and Richard Pepper Department of Communication Sciences and Disorders, Northwestern University, Frances Searle Building, 2240 Campus Drive, Evanston, IL 60208, USA. Email: jason.sanchez@northwestern.edu

## Introduction

Neurotrophins are a class of growth-factor proteins that play crucial roles in regulating normal nervous system maturation in all vertebrates.<sup>1–3</sup> Despite their ubiquity, studying neurotrophins and their corresponding tyrosine receptor kinases (Trk) has proven to be a challenge due to their complex temporal and spatial expression patterns that occur during development.<sup>4,5</sup> Such studies are further complicated by neurons' inherent heterogeneity, where neurotrophin signaling differs depending on the neuron's structure, function, and location within the nervous system.<sup>6–10</sup> However, we can partly untangle this complexity by studying the topographical organization of the chicken auditory system. Here, the frequency representation of sound (ie, tonotopic) is conserved from the peripheral to central pathways. Furthermore, the chicken also provides an excellent platform for comparative investigations on the role of neurotrophins as their auditory system relies on only 2 neurotrophins that regulate development, brain-derived neurotrophic factor (BDNF) and neurotrophin-3 (NT-3), along with their respective high-affinity receptors, TrkB and TrkC.<sup>11–16</sup>

In the peripheral auditory pathway of mice, synaptic innervation and biophysical response properties rely on BDNF and NT-3 signaling differentially along the tonotopic axis. The establishment of action potential properties in high-frequency spiral ganglion (SG) neurons are regulated by BDNF, whereas low-frequency SG neurons rely predominantly on NT-3 for establishing their correct functional phenotype.<sup>17</sup> Expression

of BDNF and NT-3 also differ; as the animal matures, BDNF expression diminishes to almost undetectable levels in rodents, while NT-3 is maintained throughout its lifetime.<sup>18</sup> In addition, BDNF and NT-3 differentially regulate calcium ( $Ca^{2+}$ ) and potassium ( $K^+$ ) currents,<sup>19–21</sup> control dendritic morphogenesis<sup>22–24</sup> and repair inner hair cell-to-SG neuronal synapses,<sup>25,26</sup> all of which are critical for normal hearing. However, aberrant neurotrophin signaling results in the spatial remodeling of the tonotopic axis in the cochlea and subsequent hearing loss,<sup>27,28</sup> while synaptic repair via neurotrophins provides a novel therapeutic approach for peripheral insult.<sup>29,30</sup> Despite this knowledge, neurotrophin function and its regulation of neuronal response properties in the central auditory pathway remain elusive.<sup>31</sup> As such, and because of the highly-organized innervation pattern of SG neurons, investigating the role of BDNF and NT-3 at a central auditory structure that receives direct input from SG neurons could provide insight to the neurotrophic effects on the auditory system as the system transitions from the peripheral to the central pathways.

Both BDNF and NT-3 ligands—along with their receptors (TrkB and TrkC, respectively)—are present at the first-order central auditory structure of gerbils<sup>32,33</sup> and the avian equivalent, nucleus magnocellularis (NM).<sup>34</sup> NM neurons have an interesting heterogeneity in their structural and functional phenotypes along the tonotopic axis that are dependent on BDNF-TrkB signaling for high-frequency neurons, which also exhibit similar expression patterns to the periphery.<sup>24</sup> However,



the role of NT-3-TrkC signaling in NM is unknown; therefore, we focused on whether NT-3-TrkC pathway has any effect on intrinsic electrophysiological properties of NM neurons, as NM is the first-order central auditory nucleus. We hypothesize that NT-3-TrkC signaling regulates the development of low-frequency NM neurons, in line with observations from peripheral SG neurons. To test this hypothesis and to determine whether functional response properties of NM neurons are dependent on neurotrophin signaling, we evaluated the effects of the NT-3/TrkC pathway before and after the onset of hearing from both high- and low-frequency regions. We found that while NT-3 had minimal effects on high-frequency NM neurons regardless of age, it did have a significant role in regulating voltage-dependent potassium ( $K_V$ ) current that shaped active and passive membrane properties for mature, low-frequency NM neurons.

## Methods

All animal procedures were performed in accordance with federal guidelines on animal welfare and approved by Northwestern University Institutional Animal Care and Use Committee. Acute brainstem slices were prepared from White Leghorn chicken (*Gallus gallus domesticus*) embryos as previously described.<sup>35–38</sup> Developmental ages for the current study were embryonic (E) days 13 and 18, corresponding to before and after hearing onset, respectively.<sup>39,40</sup> Briefly, the brainstem was dissected and isolated in ice-cold ( $\sim 0^\circ\text{C}$ ) oxygenated low- $\text{Ca}^{2+}$  high- $\text{Mg}^{2+}$  modified artificial cerebral spinal fluid (ACSF) containing the following (in mM): 130 NaCl, 2.5 KCl, 1.25  $\text{NaH}_2\text{PO}_4$ , 26  $\text{NaHCO}_3$ , 3  $\text{MgCl}_2$ , 1  $\text{CaCl}_2$ , and 10 glucose. ACSF was continuously bubbled with a mixture of 95%  $\text{O}_2$ /5%  $\text{CO}_2$  (pH 7.4, osmolarity 295–305 mOsm/L). The brainstem was blocked coronally, affixed to the stage of a vibratome slicing chamber (Dosaka Em, Ltd, Kyoto, Japan) and submerged in ice-cold ACSF. Bilaterally symmetrical coronal slices were made (250  $\mu\text{m}$  thick for E18 embryos, 300  $\mu\text{m}$  for E13) and approximately 3 to 5 slices (depending on age) containing NM were taken from caudal to rostral, roughly representing the low-to-high frequency regions, respectively. All neurons reported as caudal are taken from the first slice obtained, corresponding to the low-frequency regions of NM, while rostral neurons are taken from the last slice obtained, representing the high frequency regions of NM.

Slices were collected in a custom holding chamber and allowed to equilibrate for 2 hours at  $\sim 22^\circ\text{C}$  in normal ACSF containing the following (in mM): 130 NaCl, 2.5 KCl, 1.25  $\text{NaH}_2\text{PO}_4$ , 26  $\text{NaHCO}_3$ , 1  $\text{MgCl}_2$ , 3  $\text{CaCl}_2$ , and 10 glucose for control. For the experimental condition, NT-3 was added to the ACSF solution at the concentration of 50 ng/mL as previously described.<sup>7,41,42</sup> ACSF was continuously bubbled with a mixture of 95%  $\text{O}_2$ /5%  $\text{CO}_2$  (pH 7.4, osmolarity 295–305 mOsm/L). Slices were transferred to a recording chamber mounted on an Olympus BX51W1 (Center Valley, PA, USA) microscope for electrophysiological experiments. The microscope was equipped

with a CCD camera, 80 $\times$  water-immersion objective and infra-red differential interference contrast optics. The recording chamber was superfused continuously (Welco, Tokyo, Japan) at room temperature in oxygenated normal ACSF at a rate of 1.5 to 2 mL/min.

## Whole cell electrophysiology

Voltage- and current-clamp experiments were performed using an Axon Multiclamp 700B amplifier (Molecular Devices, Silicon Valley, CA, USA). Patch pipettes were pulled to a tip diameter of 1 to 2  $\mu\text{m}$  using a P-97 flaming/brown micropipette puller (Sutter Instrument, Novato, CA, USA) and had resistances ranging from 2 to 8 M $\Omega$ . For voltage-clamp experiments of isolated  $K_V$  currents, the internal solution contained the following (in mM): 105 K-gluconate, 35 KCl, 1  $\text{MgCl}_2$ , 10 HEPES- $\text{K}^+$ , 5 EGTA, 4 4-ATP- $\text{Mg}^{2+}$ , 0.3 4-Tris2GTP, pH adjusted to 7.3 to 7.4 with KOH. The junction potential was  $\sim -10$  mV and raw data were not corrected. Series resistance was compensated for by  $\sim 80\%$  in all voltage-clamp recordings. For current-clamp experiments, the internal solution was potassium-based and contained the following (in mM): 105 K-gluconate, 35 KCl, 1  $\text{MgCl}_2$ , 10 HEPES- $\text{K}^+$ , 5 EGTA, 4 4-ATP- $\text{Mg}^{2+}$ , and 0.3 4-Tris2GTP, pH adjusted to 7.3 to 7.4 with KOH. The junction potential was not corrected for in our current clamp experiments.

A small hyperpolarizing ( $-1$  mV, 30 ms) voltage command was presented at the beginning of each recorded trace to document and monitor whole-cell parameters (resting membrane potential (RMP), cell membrane capacitance, series resistance and input resistance). Raw data was low-pass filtered at 2 kHz and digitized at 50 kHz using a Digidata 1440A (Molecular Devices).

Pipettes were visually guided to NM. Healthy neurons were identified and distinguished from surrounding tissue based on cell morphology and location of the nucleus within the slice. It should be noted that the low affinity neurotrophin receptor, p75 ( $\text{p75}^{\text{NTR}}$ ) can be activated by all neurotrophins. However, previous reports have demonstrated that the  $\text{p75}^{\text{NTR}}$  is not expressed in chick NM<sup>34,43</sup> and activation of the  $\text{p75}^{\text{NTR}}$  is predominantly involved with neuronal death.<sup>44–46</sup> As a result, we excluded results of apoptotic neurons from the data. Apoptosis was subjectively determined by visual cues (eg, the neuronal shape, visible pyknotic nuclei, etc) and by measuring resting membrane potentials, excluding neurons with elevated levels of depolarization based on our previous reports.<sup>47–49</sup>

All experiments were conducted in the presence of a GABA<sub>A</sub>-R antagonist picrotoxin (PTX, 100  $\mu\text{M}$ ), as well as DL-2-amino-5-phosphonopentanoic acid (DL-APV, 100  $\mu\text{M}$ , an NMDA-R receptor antagonist) and 6-Cyano-7-nitroquinoxaline-2, 3-dione (CNQX, 20  $\mu\text{M}$ , an AMPA-R receptor antagonist). After a  $\text{G}\Omega$  seal was attained, membrane patches were ruptured, and NM neurons were held in whole-cell configuration for voltage-clamp recordings at membrane

potentials ranging between  $-90$  mV to  $+30$  mV. Potassium leak currents were measured offline using the averaged responses to hyperpolarizing steps from  $-80$  to  $-90$  mV as a baseline and were subtracted from the raw data. Neurons were included in the data analysis only if they had RMPs more negative than  $-50$  mV, had series resistances  $<15$  M $\Omega$ , leak currents under  $-150$  pA, and had current output less than  $+5500$  pA with the voltage held at  $+30$  mV.

Under whole-cell current clamp, we first characterized the passive intrinsic membrane properties for each age group by injecting a small hyperpolarizing current ( $-10$  pA) into the soma.<sup>48,50</sup> This paradigm minimizes the recruitment of voltage dependent ion channels that are inactive at or near rest. Membrane voltages used for data analysis were averaged over 30 repetitive trials and calculated by fitting a single exponential to the first 10 ms time window following the hyperpolarizing current injection. The membrane input resistance ( $R_M$ ) was obtained by dividing the calculated steady-state membrane voltage by the injected current. The membrane time constant ( $\tau_M$ ) was quantified by fitting a single exponential as described above and membrane capacitance ( $C_M$ ) was calculated as  $C_M = \tau_M / R_M$ .

$K_V$  channel conductances ( $G_k$ ) were obtained by the equation  $I_k = G_k (V_{MEMBRANE} - E_k)$ .  $I_k$  represents the steady-state potassium current measured in response to membrane holding voltages ( $V_{MEMBRANE}$ ). Based on our external and internal recording solutions, the reversal potential for  $K_V$  ( $E_k$ ) was  $-84$  mV.  $K_V$  channel density was calculated by normalizing isolated currents to the individual membrane capacitance ( $j_k = I_k / C$ , where  $j_k$  is the current density,  $I$  is the average current at a given membrane holding voltage, and  $C$  is the average capacitance).

For current-clamp experiments, NM neurons were held in whole-cell configuration at  $I=0$  for recording active intrinsic membrane properties. The amount of current needed to evoke an action potential developmentally changes as a function of maturation. In order to compare across different age groups, we measured action potential threshold current for each individual neuron. Action potential threshold current is defined as the minimum amount of current required for NM neurons to generate an action potential  $\sim 50\%$  of the time across 30 repetitive stimulations (interpulse stimulus intervals = 2 seconds). Once action potential threshold current was obtained, a sustained current command (duration = 100 ms) was injected into the soma at 25% above the measured threshold current for each neuron. Action potentials evoked by this current command were used to characterize active intrinsic membrane properties. In order to document neuronal excitability (ie, number of action potentials per given period of time), we injected a suprathreshold current at  $+500$  pA for 100 ms duration.

### Data analysis

Recording protocols were written and run using Clampex acquisition and Clampfit analysis software (version 10.7; Molecular Devices, Silicon Valley, CA, USA). Statistical analyses and

graphing protocols were performed using Prism (GraphPad version 8.0.2, La Jolla, CA, USA). Unpaired  $t$ -tests were used to determine significance, with Welch's correction applied for significantly differing variances. The standard for significant differences was defined as  $P < .05$ . All graphic representations of data illustrated represent the mean and standard error.

### Reagents

All bath applied drugs were allowed to perfuse through the recording chamber for  $\sim 10$  minutes before subsequent recordings. DL-APV, CNQX and all other salts and chemicals were obtained from Sigma-Aldrich (St. Louis, MO, USA). PTX was obtained from Tocris (Ellisville, MO, USA). NT-3 was obtained from Alomone Labs (Jerusalem, Israel).

### Results

To determine whether NT-3-TrkC signaling modulates electrophysiological properties and contributes to tonotopic characteristics of NM neurons, we exogenously bath-applied NT-3 to the rostral-most and the caudal-most regions of traditional NM, representing the high- and low-frequency regions respectively (ultra-low frequency NM neurons—recently termed NMc region—were not sampled<sup>47,49,51</sup>). The results in this study are based on 87 NM neurons, sampled on embryonic (E) days 13 and 18 for both the high-frequency and low-frequency neurons. Experimental NM neurons were exposed to the NT-3 ligand (50 ng/mL) added to the ACSF solution for a minimum of 2 hours before patch clamp recordings were obtained.<sup>7,41,42,52</sup> The aforementioned studies also observed acute effects of exogenous neurotrophin application in a similar temporal window.

#### NT-3 exogenous application and $K_V$ currents

The rationale for investigating  $K_V$  channels comes from numerous studies elsewhere in the brain that show neurotrophin signaling dynamically modulates (1) the phosphorylation of  $K_V$  channel properties,<sup>53</sup> (2) their intrinsic expression pattern,<sup>54</sup> and (3) their regulation of neuronal excitability.<sup>52</sup> However, it is unclear the extent to which NT-3-TrkC signaling plays a role in NM, as the aforementioned studies focused on other classes of neurotrophins and their cognate receptors from different brain regions.

Figure 1 shows representative steady-state  $K_V$  currents for control (Figure 1A) and experimental (Figure 1B, +NT-3) neurons. Steady-state  $K_V$  currents were measured across a 10 ms time window near the end of the voltage command (symbols above traces denotes sampled time periods). Bath-application of NT-3 to these high-frequency E13 NM neurons showed no effect on the modulation of steady state  $K_V$  currents. This results was consistent across the population of sampled neurons (Figure 1C), with no statistically significant change of the outward current when compared at multiple holding voltages;  $-60$  mV (Figure 1D, control,  $68.23 \pm 12.97$  pA; NT-3,  $33.53 \pm 15.06$ ;

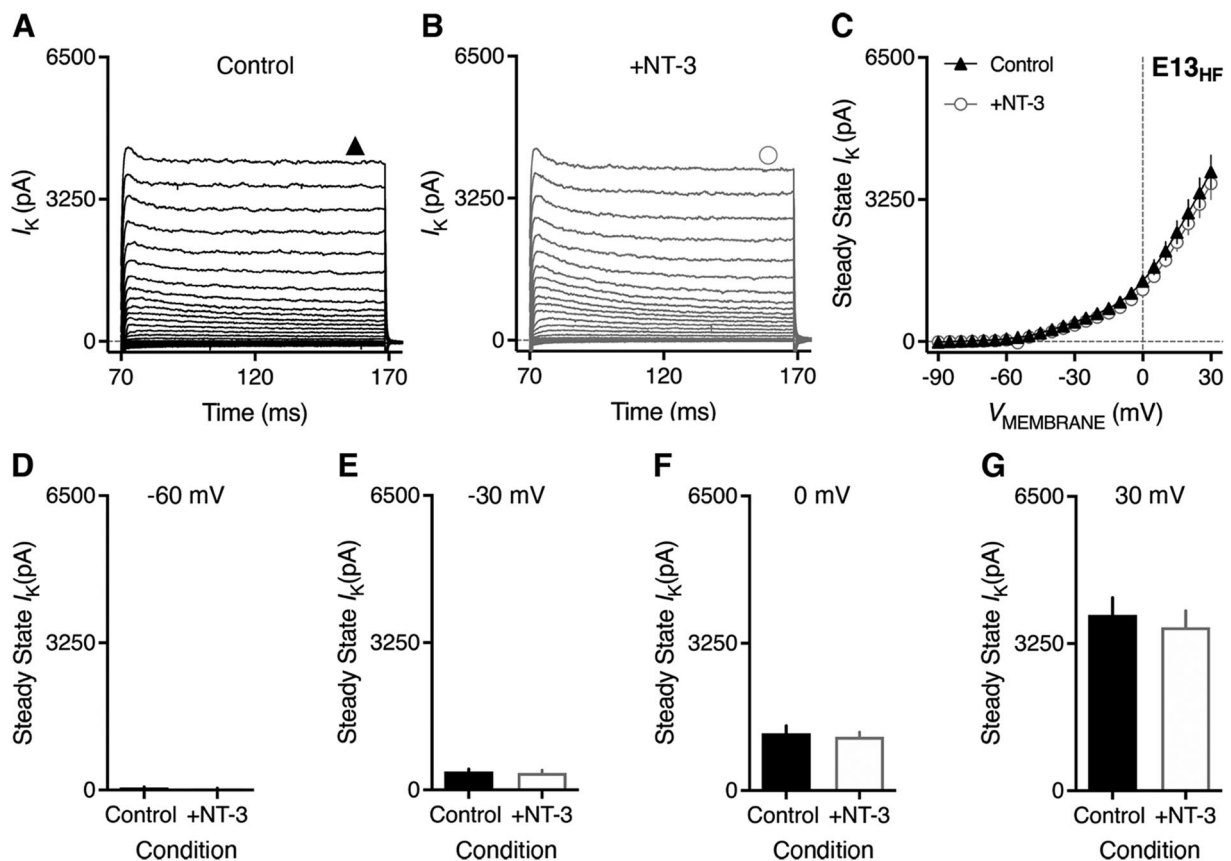


**Figure 1.**  $K_V$  current for high-frequency E13 NM neurons ( $E13_{HF}$ ). (A-B) Representative voltage-clamp traces to somatic current injections ranging from  $-90$  pA to  $+30$  pA in  $+5$  pA increments from (A) control and (B) experimental (+NT-3) NM neurons. Symbols above current traces indicate region sampled to obtain steady state potassium currents. (C) Population averaged I/V curves of control (black triangles) and the experimental (white circles) NM neurons. Data represents the mean  $\pm$  SEM. (D-G)  $K_V$  currents when the membrane voltage is held at  $-60$ ,  $-30$ ,  $0$ , and  $30$  mV. Each bar represents the mean value  $\pm$  SEM.  $N=11$  for control,  $N=9$  for NT-3.

$P=.10$ ),  $-30$  mV (Figure 1E, control,  $445.70 \pm 44.78$  pA; NT-3,  $378.18 \pm 55.35$ ;  $P=.35$ ),  $0$  mV (Figure 1F, control,  $1381.39 \pm 133.14$  pA; NT-3,  $1186.82 \pm 103.72$ ;  $P=.28$ ), and  $30$  mV (Figure 1G, control,  $3885.36 \pm 379.46$  pA; NT-3,  $3613.44 \pm 362.15$ ;  $P=.62$ ).

Bath application of NT-3 to high-frequency E18 NM neurons only slightly depressed  $K_V$  currents at the highest holding voltages. Figure 2 show representative steady-state  $K_V$  currents for control (Figure 2A) and experimental (Figure 2B) neurons. However, and similar to high-frequency E13 neurons, the modulation of the steady state  $K_V$  currents were not statistically significant at any holding voltage across the population of sampled neurons (Figure 2C);  $-60$  mV (Figure 2D, control,  $117.47 \pm 9.19$  pA; NT-3,  $117.25 \pm 10.11$ ;  $P=.99$ ),  $-30$  mV (Figure 2E, control,  $938.18 \pm 63.02$  pA; NT-3,  $856.80 \pm 75.90$ ,  $P=.41$ ),  $0$  mV (Figure 2F, control,  $2048.60 \pm 145.26$  pA; NT-3,  $1830.20 \pm 154.65$ ;  $P=.32$ ), and  $30$  mV (Figure 2G, control,  $3478.08 \pm 308.09$  pA; NT-3,  $2943.06 \pm 283.07$ ;  $P=.23$ ).

On the other hand, NT-3 application had robust effects on low-frequency E13 NM neurons. Figure 3 shows representative steady-state  $K_V$  currents for control (Figure 3A) and experimental (Figure 3B) neurons. A significant reduction of outward  $K_V$  currents was observed across multiple membrane

voltages for the population of sampled neurons (Figure 3C);  $-60$  mV (Figure 3D, control,  $79.67 \pm 10.80$  pA; NT-3,  $48.68 \pm 3.53$ ;  $P=.02$ ),  $-30$  mV (Figure 3E, control,  $393.85 \pm 34.64$  pA; NT-3,  $333.69 \pm 17.50$ ;  $P=.10$ ),  $0$  mV (Figure 3F, control,  $1300.30 \pm 122.30$  pA; NT-3,  $885.74 \pm 39.66$ ;  $P=.01$ ), and  $30$  mV (Figure 3G, control,  $3514.14 \pm 341.33$  pA; NT-3,  $2135.40 \pm 105.40$ ;  $P<.0001$ ).

Interestingly, NT-3 application had an opposite, but equally robust effect on low-frequency E18 neurons. Figure 4 shows representative steady-state  $K_V$  currents for control (Figure 4A) and experimental (Figure 4B) neurons. There was a dramatic increase in the steady-state  $K_V$  current that was heavily dependent on the membrane voltage across the population of sampled neurons (Figure 4C);  $-60$  mV (Figure 4D, control,  $88.47 \pm 10.57$  pA; NT-3,  $111.67 \pm 11.01$ ;  $P=.15$ ),  $-30$  mV, (Figure 4E, control,  $671.10 \pm 79.61$  pA; NT-3,  $1124.49 \pm 61.79$ ;  $P=.0002$ ),  $0$  mV, (Figure 4F, control,  $1575.08 \pm 207.02$  pA; NT-3,  $2724.84 \pm 133.67$ ;  $P=.0001$ ), and the largest observable increase at  $30$  mV (Figure 4G, control,  $2923.37 \pm 485.60$  pA; NT-3,  $5347.09 \pm 357.36$ ;  $P=.0007$ ).

We next addressed what factors account for the bidirectional changes in the total steady-state  $K_V$  currents for low frequency NM neurons. Such factors include the regulation of  $K_V$  channel

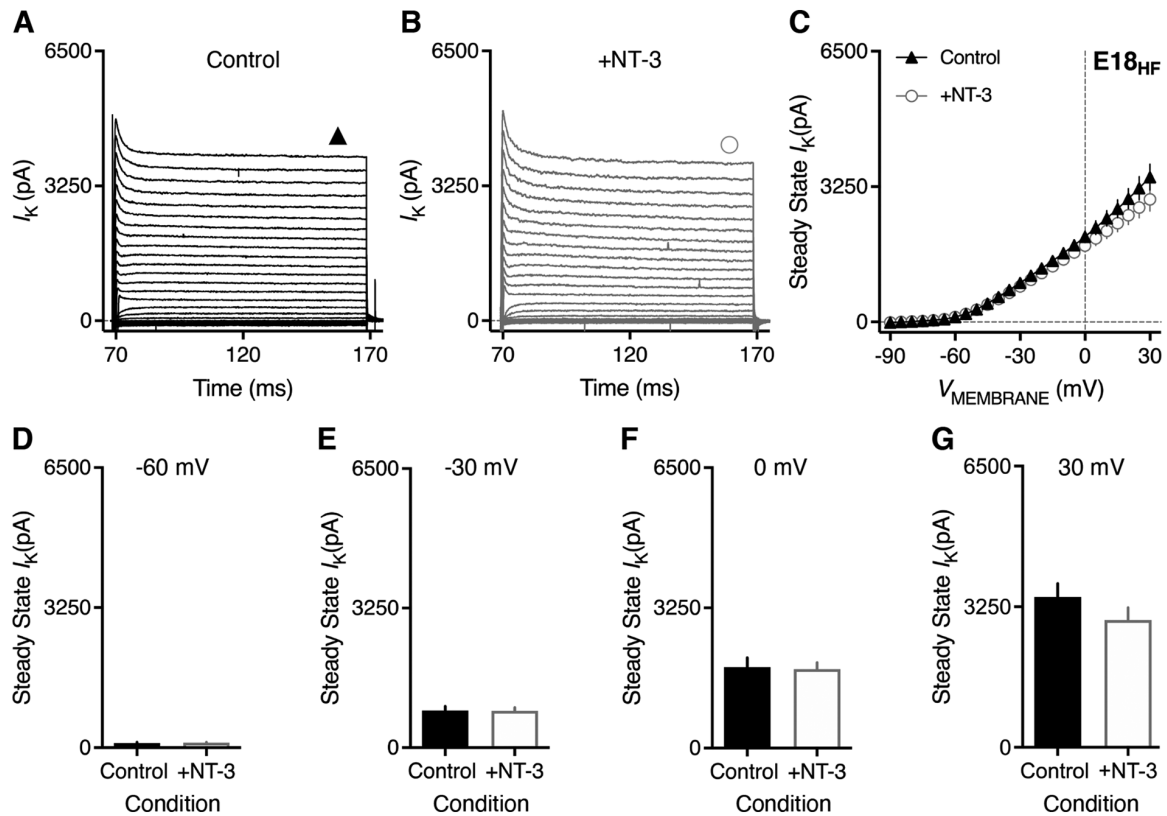


**Figure 2.**  $K_V$  current for high-frequency E18 NM neurons ( $E18_{HF}$ ). (A–B) Representative voltage-clamp traces to somatic current injections ranging from  $-90$  pA to  $+30$  pA in  $+5$  pA increments from (A) control and (B) experimental ( $+NT-3$ ) neurons. Symbols above current traces indicate region sampled to obtain steady state potassium currents. (C) Population averaged I/V curves of the control (black triangles) and experimental (white circles) NM neurons. Data represents the mean  $\pm$  SEM. (D–G)  $K_V$  currents when the membrane voltage is held at  $-60$ ,  $-30$ ,  $0$ , and  $30$  mV. Each bar represents the mean value  $\pm$  SEM.  $N=11$  for control,  $N=9$  for  $NT-3$ .

expression (channel density)—as well as—changes in  $K_V$  channel ionic flow (channel conductance). In order to identify which mechanism contributes to the changes in total steady-state  $K_V$  currents, we calculated  $K_V$  channel density and channel conductance and report them as a function of different membrane holding voltages (Figure 5, Table 1). In line with results reported for steady-state  $K_V$  channel current for both ages (Figures 3 and 4, respectively), we observed a significant decrease in  $K_V$  channel density (Figure 5A) and  $K_V$  channel conductance (Figure 5B) for low-frequency E13 NM neurons across the majority of membrane holding voltages following  $NT-3$ -application. For low-frequency E18 NM neurons, we also observed a marginal increase in  $K_V$  channel density (Figure 5C), albeit not significant at any membrane holding voltage. Conversely, we did observe a significant increase in  $K_V$  channel conductance for low-frequency E18 NM neurons following  $NT-3$  application (Figure 5D). This increase was most prominent at the highest membrane holding voltages (Table 1).

#### *NT-3 exogenous application and active membrane properties*

It is well documented that different sub-families of  $K_V$  channels regulate multiple active membrane properties as it pertains

to neuronal action potentials in the auditory system (For review, see Johnston et al<sup>55</sup>). We have previously reported that  $K_V1$ ,  $K_V2$ , and  $K_V3$  subtypes regulate neuronal excitability ( $K_V1$ ) after hyperpolarization ( $K_V2$ ) and repolarization ( $K_V3$ ) that differs across the tonotopic axis of NM.<sup>49</sup> Because bath application of  $NT-3$  affected  $K_V$  currents in an age-, voltage-, and tonotopic-dependent fashion, we predicted this would manifest itself as a regulation of neuronal repolarization, as the largest changes were observed at higher membrane voltages (eg,  $30$  mV) and for low-frequency neurons at both ages.

Figure 6 shows superimposed voltage traces for control and experimental neurons for E13 (Figure 6A) and E18 (Figure 6B) high-frequency NM neurons. In line with the lack of effect of  $NT-3$  modulation of  $K_V$  currents, the population of sampled high-frequency neurons showed no significant difference in the rate of maximum membrane voltage decay (ie, repolarization) for both E13 neurons (Figure 6C, control,  $-26.83 \pm 2.07$  mV/ms;  $NT-3$ ,  $-22.48 \pm 1.33$ ;  $P=.11$ ), and E18 neurons (Figure 6D, control,  $-113.54 \pm 7.15$  mV/ms;  $NT-3$ ,  $-99.35 \pm 6.02$ ;  $P=.15$ ). No differences were observed for the regulation of neuronal excitability (ie, an increase in the number of action potentials to sustained, suprathreshold somatic current injections), in line with the observed results for the voltage-clamp experiments (data not shown).

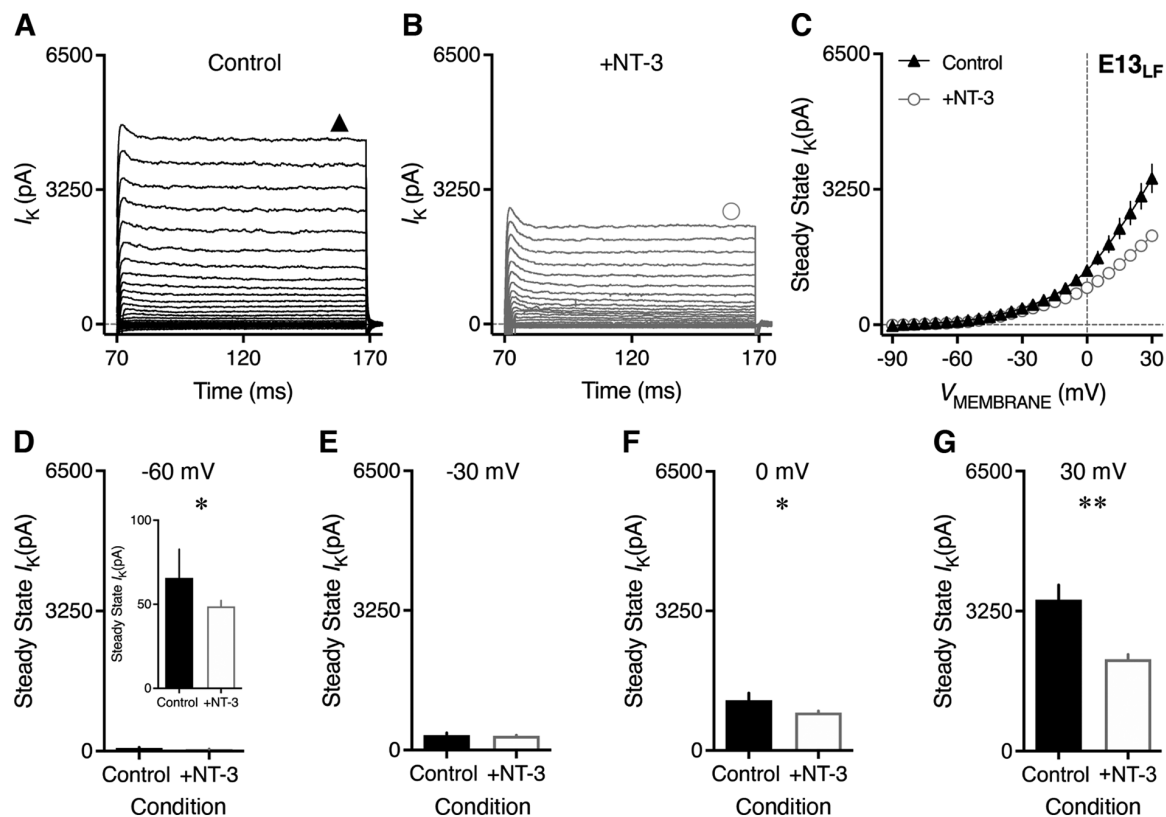


**Figure 3.**  $K_V$  current for low-frequency E13 NM neurons (E13<sub>LF</sub>). (A–B) Representative voltage-clamp traces to somatic current injections ranging from  $-90$  pA to  $+30$  pA in  $+5$  pA increments from the control (A) and experimental neurons (B). Symbols above current traces indicate region sampled to obtain steady state potassium currents. (C) Population averaged I/V curve of the control (black triangles) and experimental (white circles) NM neurons. Data represents the mean  $\pm$  SEM. (D–G)  $K_V$  currents when the membrane voltage is held at  $-60$  (inset denotes smaller scale),  $-30$ ,  $0$ , and  $30$  mV. Each bar represents the mean value  $\pm$  SEM.  $N=9$  for control,  $N=17$  for NT-3. In this and the subsequent figures,  $P$ -values as indicated: \* $<.05$ , \*\* $<.01$ , \*\*\* $<.001$ , \*\*\*\* $<.0001$ .

To our surprise, we observed no difference in membrane repolarization for low-frequency E13 neurons during NT-3 application. Figure 7A shows representative superimposed voltage traces for control and experimental low-frequency E13 neurons. This result was consistent across the population of sampled neurons (Figure 7B, control,  $-38.88 \pm 3.86$  mV/ms; NT-3,  $-36.46 \pm 2.00$ ;  $P=.54$ ), despite a significant reduction in  $K_V$  current at high membrane voltages (see Figure 3). In contrast, however, low-frequency E18 neurons showed a quickening of the action potential repolarization during NT-3 application. Figure 7C shows representative superimposed voltage traces for control and experimental low-frequency E18 neurons. This result was consistent and significant across the population of sampled neurons (Figure 7D, control,  $-76.82 \pm 10.81$  mV/ms; NT-3,  $-110.95 \pm 7.02$ ;  $P=.02$ ; Fig 6D). This result is expected given the significant increase observed for the high-voltage activated  $K_V$  currents at this age and tonotopic region of NM (see Figure 4).

#### *NT-3 exogenous application and passive membrane properties*

We have previously shown that passive membrane properties of NM neurons are highly relevant to their action potential

firing properties. Moreover, developmental changes in passive membrane properties is heavily dependent on  $K_V$  channel subunits, conductances and neuronal size.<sup>48</sup> In order to better understand the dynamic role of NT3-TrkC signaling in regulating passive membrane properties, we investigated the membrane capacitance, membrane input resistance and membrane time constant. Using whole-cell current clamp, we characterized these passive membrane properties for control and experimental neurons by applying a small hyperpolarizing somatic current injection ( $-10$  pA). The membrane voltage time constant ( $\tau_M$ ) and steady-state voltage responses were quantified by fitting a single exponential to a 10 ms time window of the voltage response following the initial current injection as we previously described.<sup>48</sup> The membrane input resistance ( $R_M$ ) was obtained by dividing the calculated steady-state voltage response to the injected current. Membrane capacitance ( $C_M$ ) was calculated based on the equation  $C_M = \tau_M/R_M$ .

There was a significant increase in neuronal membrane capacitance for high-frequency E13 NM neurons following bath application of NT-3 (Figure 8A, control,  $48.35 \pm 3.27$  pF; NT-3,  $65.40 \pm 5.07$ ;  $P=.01$ ), with minimal changes to membrane input resistance (Figure 8B, control,  $402.36 \pm 74.17$  M $\Omega$ ; NT3,

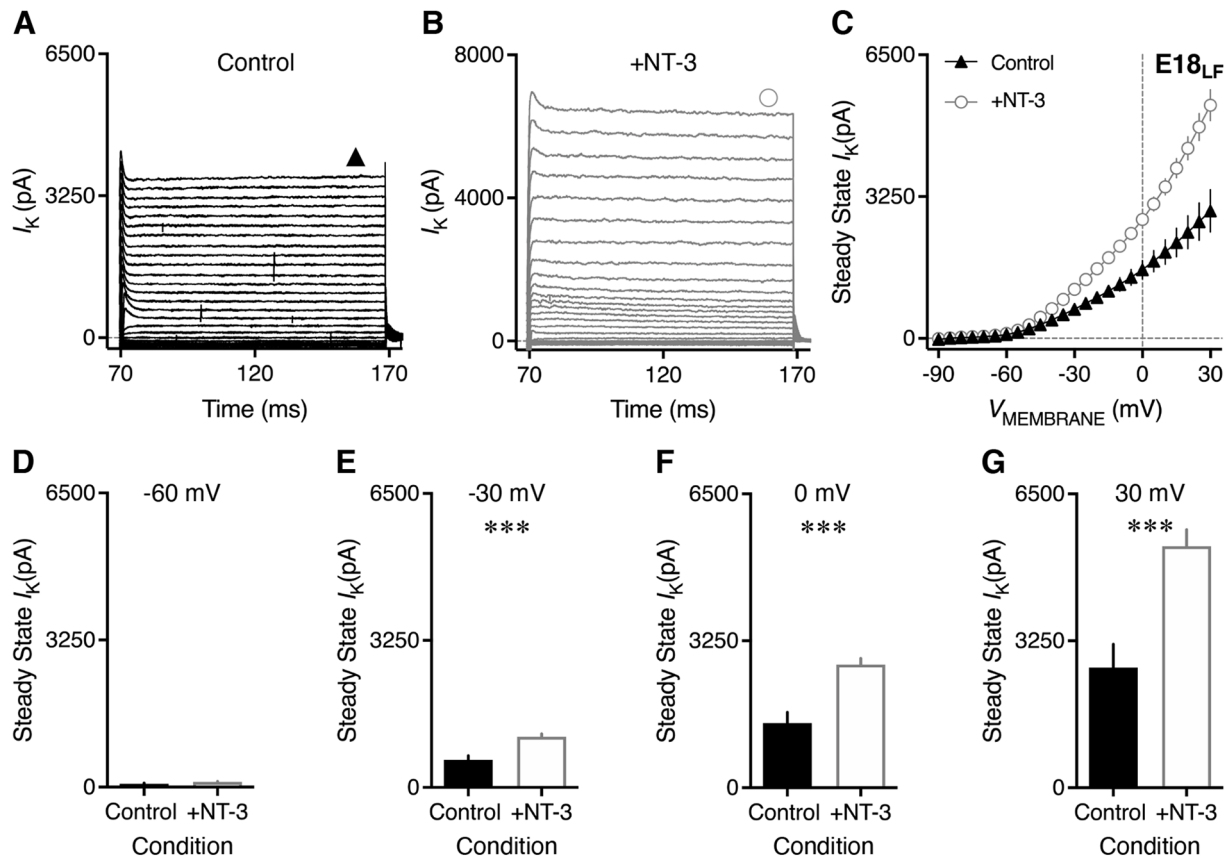


**Figure 4.**  $K_V$  current for low-frequency E18 NM neurons ( $E18_{LF}$ ). (A–B) Representative voltage-clamp traces to somatic current injections from  $-90$  pA to  $+30$  pA in  $+5$  pA increments from the control (A) and experimental (B) neurons. Symbols above current traces indicate region sampled to obtain steady state potassium currents. (C) Averaged IV curve of the control (black triangles) and the experimental (white circles) NM neuron population. Each point is mean  $\pm$  SEM. (D–G)  $K_V$  current when the voltage is held at  $-60$ ,  $-30$ ,  $0$ , and  $30$  mV. Each bar represents the mean value  $\pm$  SEM.  $N=10$  for control,  $N=11$  for NT-3.

$361.25 \pm 24.53$ ;  $P=.61$ ), and membrane voltage time constant (Figure 8C, control,  $17.93 \pm 2.52$  ms; NT-3,  $24.22 \pm 2.64$ ;  $P=.10$ ). For high-frequency E18 NM neurons, bath application of NT-3 resulted in no significant change in passive membrane properties across all parameters investigated (Figure 8D–F).

Additionally, some significant changes in passive membrane properties were observed for low-frequency NM neurons at both ages. Bath application of NT-3 for low-frequency E13 neurons resulted in a significantly larger membrane capacitance (Figure 9A, control,  $30.33 \pm 3.65$  pF; NT-3,  $42.46 \pm 9.30$ ,  $P=.007$ ) and time constant, albeit, not significant (Figure 9C, control,  $9.72 \pm 0.79$  ms; NT-3,  $12.34 \pm 1.90$ ;  $P=.21$ ). There was minimal change in membrane input resistance (Figure 9B, control,  $294.22 \pm 28.59$  M $\Omega$ ; NT-3,  $274.24 \pm 23.61$ ,  $P=.60$ ) compared to controls across the population of sampled neurons. For low-frequency E18 neurons, there were minimal changes to membrane capacitance (Figure 9D,  $20.43 \pm 4.73$  pF; NT-3,  $38.16 \pm 9.83$  pF;  $P=.13$ ) and membrane time constant (Figure 9F, control,  $3.44 \pm 0.52$  ms; NT-3,  $3.15 \pm 0.412$ ;  $P=.67$ ), but a significant reduction in membrane input resistance (Figure 9E, control,  $190.67 \pm 25.58$  M $\Omega$ ; NT-3,  $101.00 \pm 11.05$ ;  $P=.01$ ), results consistent with observed changes to the active membrane properties.

## Discussion

Despite over a century of work on the development of the vertebrate auditory system, little is known about the molecular and cellular establishment of neuronal properties in the brainstem. This is especially true regarding the role of neurotrophin ligands and their cognate receptors in regulating normal neuronal phenotypes along the frequency axis (ie, tonotopic) in the cochlear nucleus. In the auditory periphery, where the role of neurotrophins are best understood, BDNF and NT-3 signaling—via their Trk receptors—is essential for normal inner ear development, survival, tonotopy maintenance and, more recently, implicated in synaptic repair. For example, peripheral synaptopathy—a term recently coined to describe synapse damage and loss between inner hair cells and SG neurons—has been demonstrated to occur after noise exposure in animal models.<sup>56,57</sup> It has been suggested that such a loss of synaptic inputs in humans is thought to underlie auditory-related problems, including difficulties hearing speech in noisy environment.<sup>58</sup> As such, novel drug delivery methods are currently being developed in the attempt to treat and or prevent synaptopathy, and recent research suggests that specific therapeutic pathways may provide intrinsic stem-cell based therapies that target auditory-related problems in the inner ear,<sup>59</sup> including the NT-3-TrkC signaling pathway.<sup>25,26</sup>

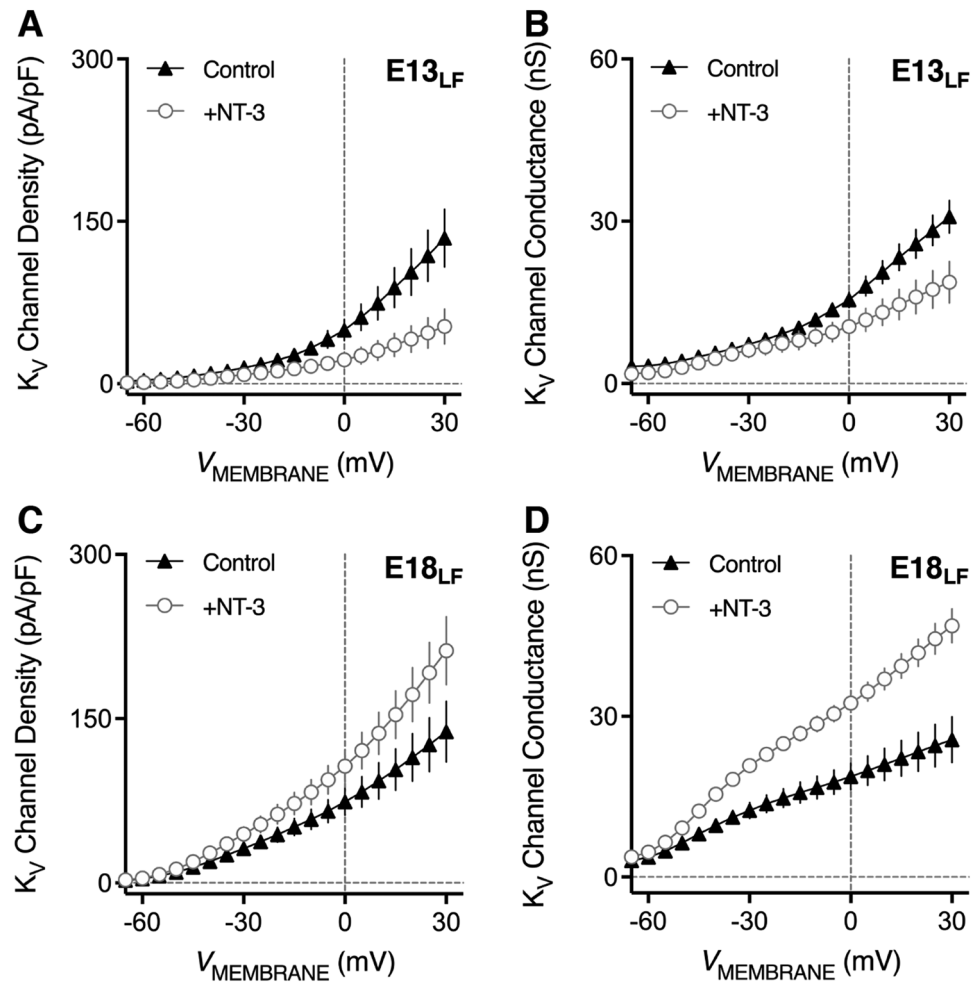


**Figure 5.**  $K_V$  channel density and conductance for low-frequency NM neurons at 2 developmental stages. Averaged  $K_V$  channel density (A) and conductance (B) plotted as a function of membrane holding voltages for low frequency E13 NM neurons (control, black triangles; experimental, white circles). Averaged  $K_V$  channel density (C) and conductance (D) plotted as a function of membrane holding voltages for low frequency E18 NM neurons (control, black triangles; experimental, white circles). Each bar represents the mean value + SEM.

**Table 1.** Measurement of  $K_V$  channel Density and Channel Conductance for Low Frequency NM neurons at E13 and E18 across different membrane holding voltages.

$K_V$ CHANNEL DENSITY (PA/PF)	E13 <sub>LF</sub>			E18 <sub>LF</sub>		
	CONTROL (9)	+NT-3 (17)	P VALUE	CONTROL (10)	+NT-3 (11)	P VALUE
-60mV	3.21 ± 2.40	1.21 ± 0.43	.04	3.87 ± 1.03	4.45 ± 2.75	.52
-30mV	14.84 ± 7.76	8.37 ± 2.80	.04	31.40 ± 14.90	44.63 ± 21.76	.12
0mV	49.54 ± 28.68	22.11 ± 6.91	.02	73.98 ± 38.34	106.7 ± 48.40	.10
30mV	134.60 ± 79.70	52.94 ± 15.95	.02	138.17 ± 87.65	212.02 ± 103.00	.09
$K_V$ CHANNEL CONDUCTANCE (NS)	CONTROL (9)	+NT-3(17)	P VALUE	CONTROL (10)	+NT-3 (11)	P VALUE
	-60mV	3.32 ± 1.35	2.03 ± 0.61	.02	3.69 ± 1.39	4.65 ± 1.52
-30mV	7.29 ± 1.92	6.18 ± 1.34	.10	12.43 ± 4.66	20.82 ± 3.80	.0002
0mV	15.48 ± 4.37	10.54 ± 1.95	.009	18.75 ± 7.79	32.44 ± 5.28	.0001
30mV	30.83 ± 8.98	18.73 ± 3.81	.003	25.64 ± 13.47	46.90 ± 10.40	.0007

Numerical data values represent mean ± 1 standard deviation. Numbers in parenthesis=Number of sampled neurons (N).



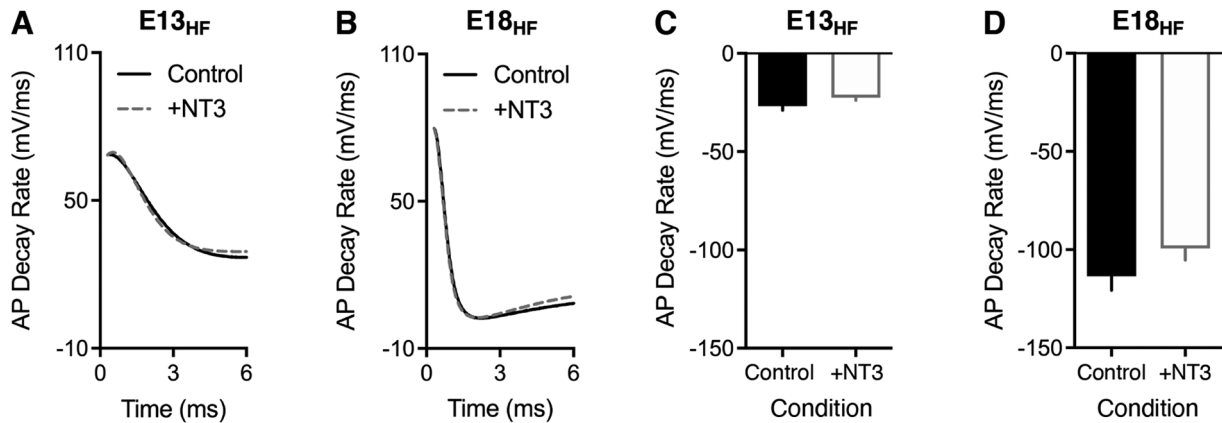


**Figure 6.** Active membrane properties for high-frequency NM neurons at 2 developmental stages. (A–B) Superimposed repolarization voltage traces for E13 (A) and E18 (B) high-frequency NM neurons to a somatic current injection 25% above action potential firing threshold. Voltage traces are representative of the population. (C–D) Maximum decay rates of action potential repolarization for E13 (C) and E18 (D) high-frequency NM neurons. Each bar represents the mean value + SEM.

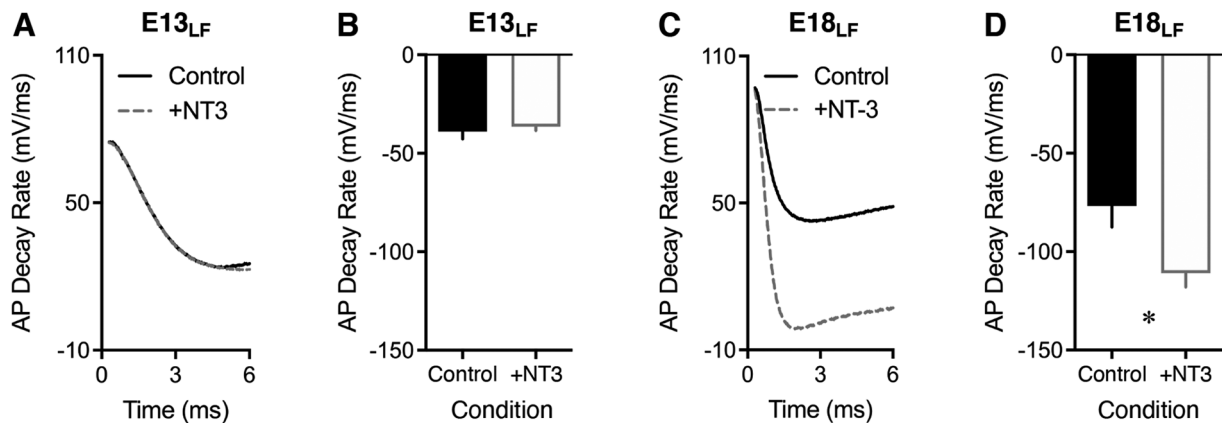


**Figure 7.** Active membrane properties for low-frequency NM neurons at 2 developmental stages. (A–B) Superimposed repolarization voltage traces for E13 (A) and E18 (B) low-frequency NM neurons to a somatic current injection 25% above action potential firing threshold. Voltage traces are representative of the population. (C–D) Maximum decay rates of action potential repolarization for E13 (C) and E18 (D) low-frequency NM neurons. Each bar represents the mean value + SEM.

While neurotrophins in the development of the peripheral auditory system has been studied extensively for over 2 decades, their functional role in the developing central system remains elusive.<sup>31</sup> Because neurotrophins' transcellular transport can span long physical distances,<sup>3</sup> it is intriguing to consider that NT-3 delivery to the inner ear can target central neuronal circuits. Identifying the functional role of NT-3-TrkC signaling during pre- and post-hearing periods is timely and essential; providing a solid foundation for the development and efficiency of such therapeutic methods.

In this study we investigated the effects of NT-3-TrkC signaling on intrinsic properties of neurons in the avian cochlear NM, the first central nuclei to receive inputs from peripheral SG neurons. We predicted that, since NT-3-TrkC activation contributes to the functional regulation of low-frequency SG neurons, it would have the same effect on low-frequency NM neurons because of the precise topographical connectivity in the auditory system. In line with the lack of NT-3-TrkC contribution to high frequency SG neurons response properties, we further predicated

that NM neurons located in the high-frequency region of the nucleus would not be affected. Largely due to the observation that BDNF-TrkB signaling is the primary expression pattern found in high-frequency NM.<sup>34</sup> Indeed, we observed minimal change in current and voltage responses from high-frequency NM neurons when the NT-3 ligand was exogenously bath applied to brainstem tissue. In contrast, we observed robust and temporally dynamic changes in low-frequency neurons, such as the bidirectional modification of  $K_V$  currents before and after hearing onset. This, in turn, affected the hyperpolarizing membrane voltage by decreasing decay rate when  $K_V$  currents were suppressed (E13), or increasing decay rate when  $K_V$  currents were enhanced (E18). These results indicate that NT-3 has a robust effect on low-frequency neurons. In addition, and as previously noted, the low affinity p75<sup>NTR</sup> has not been observed in NM<sup>34,43</sup> and its principal role involves apoptosis.<sup>44–46</sup> Therefore, we assume that only NT-3-TrkC signaling dominates in low-frequency NM and the effects seen here by the exogenous application of NT-3 was triggered by the activation of TrkC receptors.

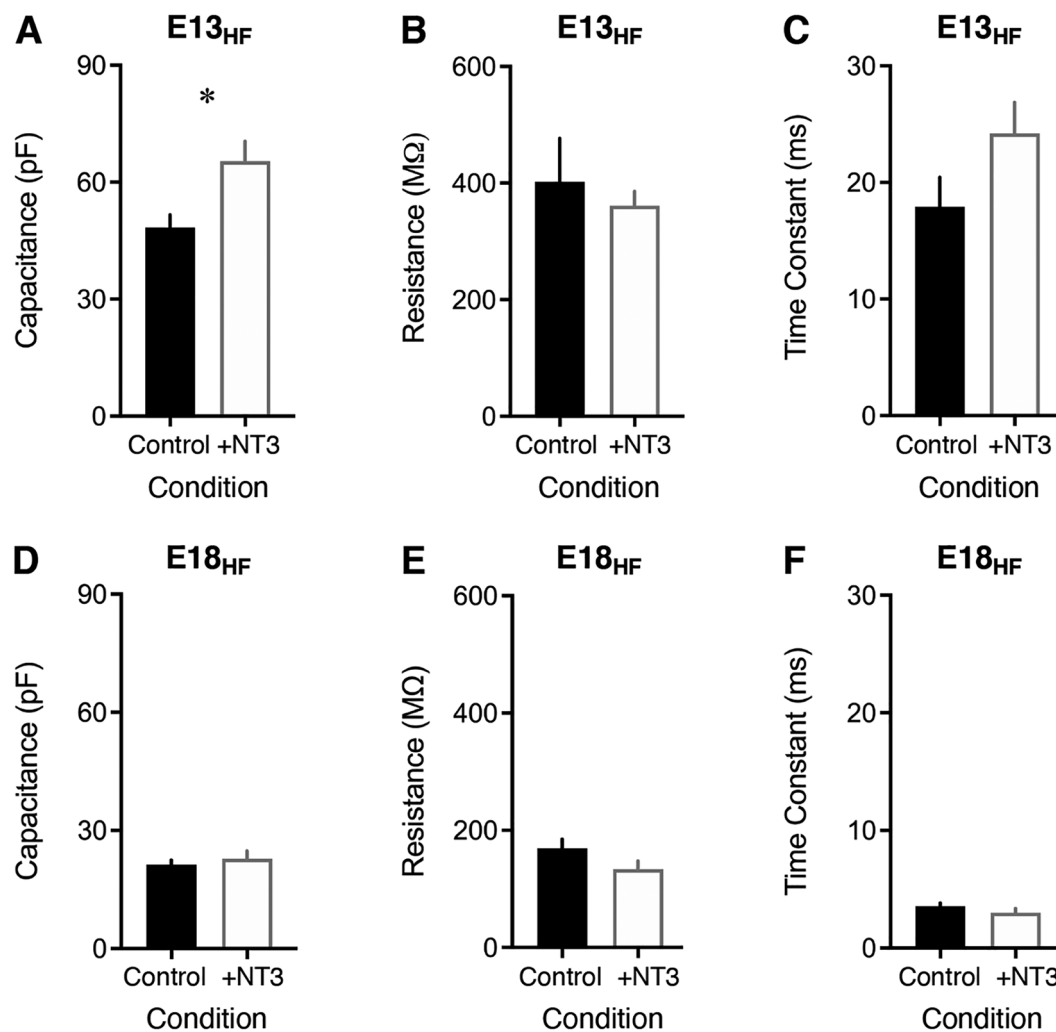


**Figure 8.** Passive membrane properties for high-frequency NM neurons at 2 developmental stages. (A) Membrane capacitance ( $\tau_m/R_m$ ), (B) membrane resistance ( $R_m$ ), and (C) membrane time constant ( $\tau_m$ ) for E13 high-frequency NM neurons. (D) Membrane capacitance ( $\tau_m/R_m$ ), (E) membrane resistance, and (F) membrane time constant ( $\tau_m$ ) for E18 high-frequency neurons. Each bar represents the mean value + SEM.

Specifically, NT-3 bath application and its subsequent activation of TrkC receptors resulted in a bidirectional change in  $K_V$  currents for both ages, but only in the low-frequency region.  $K_V$  currents were reduced at E13 but enhanced for E18, the latter of which resulted in a quickening of the action potential repolarizing phase, an expected result consistent with an increase in  $K_V3$ -containing channels. We expected the inverse to happen, with the reduced  $K_V$  currents slowing down the repolarizing phase. Surprisingly, this was not observed for E13 low-frequency neurons; reduction in  $K_V$  current resulted in minimal change for action potential repolarization. We attribute this unexpected result to basal levels of change in  $K_V$  currents that differed between E13 and E18, as E18  $K_V$  current had nearly 100% difference between the control and NT-3 population while at E13 the percent-fold difference was merely 50%. It is therefore conceivable that this percent-fold change was not enough to establish a significant difference in action potential repolarization rates. Alternatively, other intrinsic ion channel properties— independent of  $K_V3$ -containing channels—are responsible for action potential repolarization in low frequency

13 NM neurons (eg,  $K_V2$  containing channels). Future work could address this alternative issue.

The overall shape of the membrane voltage responses also changed between pre- and post-hearing onset. It has been previously documented that younger embryos have less low-voltage activated potassium channels ( $K_{LVA}$ ) with minimal  $K_V1$  channel contribution.<sup>48,60</sup> Lack of  $K_V1$  contributes to the initiation of subsequent neuronal depolarization that results in repetitive AP firing to sustained inputs; here, we observed a similar pattern in some neuron regardless of whether NT-3 was bath-applied (data not shown). Interestingly, while high- and low-frequency neurons cannot be distinguished by the voltage responses before hearing onset, there is a clear difference post-hearing onset. If endogenous NT-3 had already initiated the tonotopic differentiation before hearing onset, control neurons would show differences between high-frequency and low-frequency neurons. Therefore, this indistinguishable result between high-frequency and low-frequency neurons suggest that unlike SG neurons,<sup>17</sup> tonotopy and intrinsic property refinement are established post-hearing

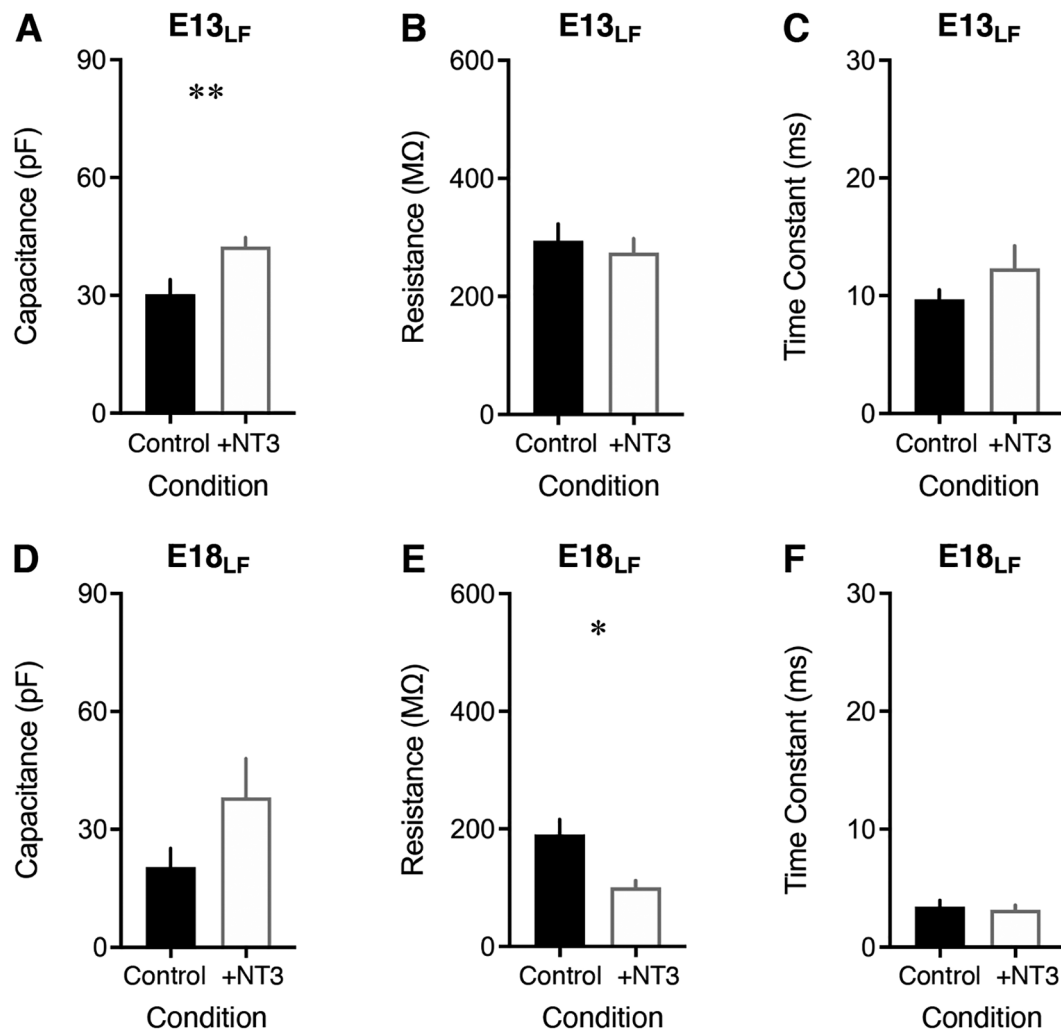


**Figure 9.** Passive membrane properties for low-frequency neurons at 2 developmental stages. (A) Membrane capacitance ( $\tau_M/R_M$ ), (B) membrane resistance ( $R_M$ ), and (C) membrane time constant ( $\tau_M$ ) for E13 low-frequency NM neurons. (D) Membrane capacitance ( $\tau_M/R_M$ ), (E) membrane resistance, and (F) membrane time constant ( $\tau_M$ ) for E18 low-frequency NM neurons. Each bar represents the mean value + SEM.

onset via NT-3 anterograde transport from peripheral SG neurons to central auditory structures.

If we consider the developmental expression of TrkC in the periphery<sup>17</sup> and the documented effects of neurotrophins on  $K_V$  channels,<sup>53,61</sup> the explanation that NT-3 increased  $K_V3$  and  $K_V1$ -containing channel expression seems plausible. However, another explanation that deserves consideration is the possibility that the NT-3-TrkC signaling affects not only  $K_V$  channel expression, but also its open probability as well. While the effect of neurotrophins on ion channel probability has only been observed in  $Ca^{2+}$  channels,<sup>62</sup> one compelling reason to consider changes in open probability is that altering open probability requires less time than altering channel expression. Considering that the changes in macroscopic  $K_V$  current involves both channel density and its open probability, it is likely therefore that NT-3-TrkC signaling alters both.

Indeed, we observed bidirectional changes in  $K_V$  channel density and  $K_V$  channel conductance that were in agreement with changes in  $K_V$  channel steady-state current when NT-3 was exogenously applied. Before the onset of hearing (E13),

low-frequency NM neurons showed a significant reduction in  $K_V$  channel density and  $K_V$  channel conductance, while an increase in both properties were observed post hearing onset (E18) for low-frequency NM neurons, with significantly larger changes observed for  $K_V$  channel conductance versus density for E18 neurons. These results suggest that the number of available  $K_V$  channels and their subsequent open-probability to ionic flow are differentially and dynamically regulated by NT-3-TrkC signaling during embryonic development for low-frequency NM neurons. The functional relevance of the bidirectional regulation of NT-3-TrkC signaling during development remains to be determined and future studies are aimed at addressing this issue.

This study focused on the effect of NT-3-TrkC signaling on  $K_V$  currents. Although we had observed some changes in the maximum rise rate of the membrane voltage response, we did not block  $Na^+$  channels to investigate whether this change was due to NT-3-TrkC signaling affecting  $Na^+$  channels or whether it was by some other unknown mechanism, and this still remains to be investigated. What is known is that NT-3-TrkC

signaling does help regulate  $\text{Na}^+$  current density in hippocampal neurons,<sup>63</sup> and therefore it is possible that NT-3-TrkC signaling affects  $\text{Na}^+$  channels in the central auditory system. Recent reports also demonstrate that NT-3-TrkC alters neuronal excitability in the hippocampus by moving the axon initial segment closer to the soma,<sup>9</sup> which contribute to changes in action potential properties. Whether NT-3-TrkC contributes to dendritic proliferation in the central auditory system has not yet been determined. At this point we can only conjecture that the membrane changes observed by the passive properties (discussed further below) are due to dendritic proliferation; however, NT-3-TrkC does contribute to robust proliferation of dendritic arborization in Purkinje cells.<sup>23</sup>

We also observed a slight increase in membrane capacitance for low-frequency NM neurons that were age dependent (ie, E18), suggesting a larger neuronal membrane surface area accompanied by dendritic outgrowth. This suggestion has been supported by our previous work that shows genetically modified NM neurons that continually express TrkB receptors maintain elaborate dendritic architecture.<sup>24</sup> These results may also contribute to the dramatic increase of the  $\text{K}_V$  current at E18 if we posit that  $\text{K}_V$  channels, which are present in NM,<sup>64-66</sup> can also be located on the dendrites and their subsequent outgrowth. Similarly, the change in membrane input resistance can also be attributed to altered  $\text{K}_V$  channel conductance and density on the neuronal membrane surface, or the possibility that the open probability is altered because of the NT-3/TrkC pathway activation, or the combination of the 2. If open probability is altered because of the activation, then this would allow more channels to be open at lower voltages, thereby resulting in a lower membrane input resistance. Either way, the lower membrane input resistance could result from more open channels.

## Conclusion and Functional Relevance

NT-3 has temporally and structurally dynamic roles in establishing a functional nervous system, that range from altering intrinsic properties and synaptic transmission<sup>67</sup> to controlling calcium channels that contribute to synaptic transmission,<sup>62</sup> of which the subtype L-type is required to maintain auditory brainstem nuclei.<sup>68</sup> Morphological as well as electrophysiological investigations must be performed in order to get a more complete picture of the role of NT-3 in establishing and maintaining a functional central auditory system. Despite this need, there are gaps in knowledge in the developmental profiling of all neurotrophins in the central auditory system. Since it is possible that afferent SG neurons of the peripheral auditory system are an avenue for transporting neurotrophins to the central system, any external application of neurotrophins to the periphery may affect central circuits. It should be noted, however, that glial cells do contribute to central auditory brainstem development and its functional circuitry.<sup>69,70</sup> Since glial cells do produce NT-3,<sup>71</sup> the specific source of NT-3 for the central auditory pathway remains to be determined. What we have shown here is that NT-3 does have robust and bidirectional effects on

intrinsic neuronal properties, including  $\text{K}_V$  currents and active and passive membrane properties of low-frequency NM neurons. This is especially true for the modification of  $\text{K}_V$  currents and is similar to known NT-3 effects on low-frequency SG neurons of the auditory peripheral. Future work will investigate the relative functional contribution of NT-3 sodium channel currents and synaptic transmission throughout embryonic development.


## Acknowledgements

We thank George Ordiway and James McQuaid for editing a previous version of the manuscript.

## Author Contributions

MT and JTS designed experimental protocols. MT performed experiments and collected data. MT and JTS analyzed and interpreted the data. MT and JTS wrote the manuscript.

## ORCID iDs

Momoko Takahashi  <https://orcid.org/0000-0003-3816-6025>

Jason Tait Sanchez  <https://orcid.org/0000-0002-2963-3771>

## REFERENCES

- Lewin GR, Barde Y-A. Physiology of the neurotrophins. *Annu Rev Neurosci.* 1996;19:289-317.
- Snider WD. Functions of the neurotrophins during nervous system development: what the knockouts are teaching us. *Cell.* 1994;77:627-638.
- Huang EJ, Reichardt LF. Neurotrophins: roles in neuronal development and function. *Annu Rev Neurosci.* 2001;24:677-736.
- Nikoletopoulou V, Lickert H, Frade JM, et al. Neurotrophin receptors TrkA and TrkC cause neuronal death whereas TrkB does not. *Nature.* 2010;467:59-63.
- Arévalo JC, Wu SH. Neurotrophin signaling: many exciting surprises! *Cell Mol Life Sci.* 2006;63:1523-1537.
- Huang EJ, Reichardt LF. Trk receptors: roles in neuronal signal transduction. *Annu Rev Biochem.* 2003;72:609-642.
- Henion PD, Garner AS, Large TH, Western JA. Trk C-mediated NT-3 signaling is required for the early development of a subpopulation of neurogenic neural crest cells. *Dev Biol.* 1995;172:602-613.
- Shimazu K, Zhao M, Sakata K, et al. NT-3 facilitates hippocampal plasticity and learning and memory by regulating neurogenesis. *Learn Mem.* 2006;13:307-315.
- Guo Y, Su Z, Chen Y, Chai Z. Brain-derived neurotrophic factor/neurotrophin 3 regulate axon initial segment location and affect neuronal excitability in cultured hippocampal neurons. *J Neurochem.* 2017;142(2):260-271.
- Fujishima K, Kawabata Galbraith K, Kengaku M. Dendritic self-avoidance and morphological development of cerebellar purkinje cells. *Cerebellum.* Published online October 1, 2018. doi:10.1007/s12311-018-0984-8
- Fritzsch B, Barbacid M, Silos-Santiago I. The combined effects of trkB and trkC mutations on the innervation of the inner ear. *Int J Dev Neurosci.* 1998;16:493-505.
- Barbacid M. The Trk family of neurotrophin receptors. *J Neurobiol.* 1994;25:1386-1403.
- Reichardt LF. Neurotrophin-regulated signalling pathways. *Philos Trans R Soc Lond B Biol Sci.* 2006;361:1545-1564.
- Pirvola U, Ylikoski J, Palgi J, Lehtonen E, Arumäe U, Saarma M. Brain-derived neurotrophic factor and neurotrophin 3 mRNAs in the peripheral target fields of developing inner ear ganglia. *Proc Natl Acad Sci USA.* 1992;89:9915-9919.
- Ylikoski J, Pirvola U, Moshnyakov M, Palgi J, Arumäe U, Saarma M. Expression patterns of neurotrophin and their receptor mRNAs in the rat inner ear. *Hear Res.* 1993;65:69-78.
- Wheeler EF, Bothwell M, Schecterson LC, von Bartheld CS. Expression of BDNF and NT-3 mRNA in hair cells of the organ of Corti: quantitative analysis in developing rats. *Hear Res.* 1994;73:46-56.
- Adamson CL, Reid MA, Davis RL. Opposite actions of brain-derived neurotrophic factor and neurotrophin-3 on firing features and ion channel composition of murine spiral ganglion neurons. *J Neurosci.* 2002;22:1385-1396.

18. Chen H, Shi L, Liu L, Yin S, Aiken S, Wang J. Noise-induced cochlear synaptopathy and signal processing disorders. *Neuroscience*. Published online 2019. doi:10.1016/j.neuroscience.2018.09.026
19. Jiménez C, Giráldez F, Represa J, García-Díaz J. Calcium currents in dissociated cochlear neurons from the chick embryo and their modification by neurotrophin-3. *Neuroscience*. 1997;77:673-682.
20. García-Díaz JF. Development of a fast transient potassium current in chick cochlear ganglion neurons. *Hear Res*. 1999;135:124-134.
21. Kimitsuki T, Nakashima T, Kawano H, Komune S. Neurotrophin-3 modifies potassium currents in isolated inner hair cells from guinea-pig cochlea. *Auris Nasus Larynx*. 2003;30(2):141-145.
22. Zagrebelsky M, Gödecke N, Remus A, Korte M. Cell type-specific effects of BDNF in modulating dendritic architecture of hippocampal neurons. *Brain Struct Funct*. 2018;0:0. doi:10.1007/s00429-018-1715-0
23. Joo W, Hippenmeyer S, Luo L. Dendrite morphogenesis depends on relative levels of NT-3/TrkC signaling. *Science (80- )*. 2014;346:626-629.
24. Schecterson LC, Sanchez JT, Rubel EW, Bothwell M. TrkB downregulation is required for dendrite retraction in developing neurons of chicken nucleus magnocellularis. *J Neurosci*. 2012;32:14000-14009.
25. Chen H, Xing Y, Xia L, Chen Z, Yin S, Wang J. AAV-mediated NT-3 overexpression protects cochlea against noise-induced synaptopathy. *Gene Ther*. Published online March 13, 2018. doi:10.1038/s41434-018-0012-0
26. Lee MY, Kurioka T, Nelson MM, et al. Viral-mediated Ntf3 overexpression disrupts innervation and hearing in nondefened guinea pig cochlea. *Mol Ther - Methods Clin Dev*. 2016;3:16052. doi:10.1038/mtm.2016.52
27. Fariñas I, Jones KR, Tessarollo L, et al. Spatial shaping of cochlear innervation by temporally regulated neurotrophin expression. *J Neurosci*. 2001;21:6170-6180. Accessed May 22, 2019. <http://www.ncbi.nlm.nih.gov/pubmed/11487640>
28. Schimmang T, Tan J, Müller M, et al. Lack of Bdnf and TrkB signalling in the postnatal cochlea leads to a spatial reshaping of innervation along the tonotopic axis and hearing loss. *Development*. 2003;130:4741-4750.
29. Youm I, Li W. Cochlear hair cell regeneration: an emerging opportunity to cure noise-induced sensorineural hearing loss. *Drug Discov Today*. 2018;23:1564-1569.
30. Wan G, Gómez-Casati ME, Gigliello AR, Liberman MC, Corfas G. Neurotrophin-3 regulates ribbon synapse density in the cochlea and induces synapse regeneration after acoustic trauma. *Elife*. 2014;3:1-35.
31. Fritsch B, Tessarollo L, Coppola E, Reichardt LF. Neurotrophins in the ear: their roles in sensory neuron survival and fiber guidance. *Prog Brain Res*. 2004;146:265-278.
32. Hafidi A. Distribution of BDNF, NT-3 and NT-4 in the developing auditory brainstem. *Int J Dev Neurosci*. 1999;17:285-294.
33. Hafidi A, Moore T, Sanes DH. Regional distribution of neurotrophin receptors in the developing auditory brainstem. *J Comp Neurol*. 1996;367:454-464.
34. Cochran SL, Stone JS, Bermingham-McDonogh O, Akers SR, Lefcort F, Rubel EW. Ontogenetic expression of trk neurotrophin receptors in the chick auditory system. *J Comp Neurol*. 1999;413:271-288.
35. Sanchez JT, Wang Y, Rubel EW, et al. Development of glutamatergic synaptic transmission in binaural auditory neurons. *J Neurophysiol*. 2010;104:1774-1789.
36. Sanchez JT, Seidl AH, Rubel EW, Barria A. Control of neuronal excitability by NMDA-type glutamate receptors in early developing binaural auditory neurons. *J Physiol*. 2012;590:4801-4818.
37. Sanchez JT, Seidl AH, Rubel EW, Barria A. Preparation and culture of chicken auditory brainstem slices. *J Vis Exp*. 2011;34:4914-4919.
38. Sanchez JT, Quinones K, Otto-Meyer S. Factors influencing short-term synaptic plasticity in the avian cochlear nucleus magnocellularis. *J Exp Neurosci*. 2015;2015(suppl 2):11-24.
39. Jones TA, Jones SM, Paggett KC, Paggett Emer KC. Emergence of Hearing in the Chicken Embryo. *J Neurophysiol*. 2006;96:128-141.
40. Saunders JC, Coles RB, Richard Gates G. The development of auditory evoked responses in the cochlea and cochlear nuclei of the chick. *Brain Res*. 1973;63:59-74.
41. Needham K, Nayagam BA, Minter RL, O'Leary SJ, Leary SJO. Combined application of brain-derived neurotrophic factor and neurotrophin-3 and its impact on spiral ganglion neuron firing properties and hyperpolarization-activated currents. *Hear Res*. 2012;291:1-14.
42. Ichim G, Genevois A-L, Me Nard M, et al. The dependence receptor trkC triggers mitochondria-dependent apoptosis upon Cobra-1 recruitment. *Mol Cell*. 2013;51:632-646.
43. Cramer KS, Karam SD, Bothwell M, Cerretti DP, Pasquale EB, Rubel EW. Expression of EphB receptors and ephrinB ligands in the developing chick auditory brainstem. *J Comp Neurol*. 2002;452:51-64.
44. Barker PA. p75NTR Is Positively Promiscuous. *Neuron*. 2004;42:529-533.
45. Bhakar AL, Howell JL, Paul CE, et al. Apoptosis induced by p75NTR overexpression requires jun kinase-dependent phosphorylation of bad. *J Neurosci*. 2003;23:11373-11381.
46. Bredesen DE, Rabizadeh S. p75NTR and apoptosis: Trk-dependent and Trk-independent effects. *Trends Neurosci*. 1997;20:287-291.
47. Hong H, Wang X, Lu T, Zorio DAR, Wang Y, Sanchez JT. Diverse intrinsic properties shape functional phenotype of low-frequency neurons in the auditory brainstem. *Front Cell Neurosci*. 2018;12.
48. Hong H, Rollman L, Feinstein B, Sanchez JT. Developmental profile of ion channel specializations in the avian nucleus magnocellularis. *Front Cell Neurosci*. 2016;10:80.
49. Hong H, Sanchez JT. Need for speed and precision: structural and functional specialization in the cochlear nucleus of the avian auditory system. *J Exp Neurosci*. 2018;12.
50. Franzen DL, Gleiss SA, Berger C, Kümpfbeck FS, Ammer JJ, Felmy F. Development and modulation of intrinsic membrane properties control the temporal precision of auditory brain stem neurons. *J Neurophysiol*. 2015;113:524-536.
51. Wang X, Hong H, Brown DH, Sanchez JT, Wang Y. Distinct neural properties in the low-frequency region of the chicken cochlear nucleus magnocellularis. *eneuro*. 2017;4:ENEURO.0016-17.2017.
52. Youssofian M, Walmsley B. Brain-derived neurotrophic factor modulates cell excitability in the mouse medial nucleus of the trapezoid body. *Eur J Neurosci*. 2007;25:1647-1652.
53. Tucker K, Fadool DA. Neurotrophin modulation of voltage-gated potassium channels in rat through TrkB receptors is time and sensory experience dependent. *J Physiol*. 2002;542:413-429.
54. Leng J, Jiang L, Chen H, Zhang X. Brain-derived neurotrophic factor and electrophysiological properties of voltage-gated ion channels during neuronal stem cell development. *Brain Res*. 2009;1272:14-24.
55. Johnston J, Forsythe ID, Kopp-Scheinpflug C. Symposium review: going native: voltage-gated potassium channels controlling neuronal excitability. *J Physiol*. 2010;588:3187-3200.
56. Kujawa SG, Liberman MC. Adding insult to injury: cochlear nerve degeneration after "temporary" noise-induced hearing loss. *J Neurosci*. 2009;29:14077-14085.
57. Kujawa SG, Liberman MC. Synaptopathy in the noise-exposed and aging cochlea: Primary neural degeneration in acquired sensorineural hearing loss. *Hear Res*. 2015;330:191-199.
58. Kobel M, Le Prell CG, Liu J, Hawks JW, Bao J. Noise-induced cochlear synaptopathy: Past findings and future studies. *Hear Res*. 2017;349:148-154.
59. Almeida LGD, Cruz DB da, Mingroni Netto RC, Batissoco AC, Ferraz JOR, Silva RS. Stem-cell therapy for hearing loss: are we there yet? *Braz J Otorhinolaryngol*. 2019;85:520-529.
60. Akter N, Adachi R, Kato A, Fukaya R, Kuba H. Auditory input shapes tonotopic differentiation of Kv1.1 expression in avian cochlear nucleus during late development. *J Neurosci*. 2018;38:2967-2980.
61. Wright T, Gillespie LN, O'Leary SJ, Needham K, O'Leary SJ, Needham K. Firing frequency and entrainment maintained in primary auditory neurons in the presence of combined BDNF and NT3. *Sci Rep*. 2016;6:28584.
62. Baldelli P, Forni PE, Carbone E. BDNF, NT-3 and NGF induce distinct new Ca<sup>2+</sup> channel synthesis in developing hippocampal neurons. *Eur J Neurosci*. 2000;12:4017-4032.
63. Igelhorst BA, Niederkinkhaus V, Karus C, Lange MD, Dietzel ID. Regulation of neuronal excitability by release of proteins from glial cells. *Philos Trans R Soc B Biol Sci*. 2015;370:20140194.
64. Parameshwaran S, Carr CE, Perney TM. Expression of the Kv3.1 potassium channel in the avian auditory brainstem. *J Neurosci*. 2001;21:485-494. Accessed May 22, 2019. <http://www.jneurosci.org/content/jneuro/21/2/485.full.pdf>
65. Parameshwaran-Iyer S, Carr CE, Perney TM. Localization of KCNC1 (Kv3.1) potassium channel subunits in the avian auditory nucleus magnocellularis and nucleus laminaris during development. *Published online* 2003. doi:10.1002/neu.10198
66. Lu Y, Monsivais P, Tempel BL, Rubel EW. Activity-Dependent Regulation of the Potassium Channel Subunits Kv1.1 and Kv3.1. *J Comp Neurol*. 2004;470:93-106.
67. Sun W, Salvi RJ. Brain derived neurotrophic factor and neurotrophic factor 3 modulate neurotransmitter receptor expressions on developing spiral ganglion neurons. *Neuroscience*. 2009;164:1854-1866.
68. Ebbers L, Satheesh S V, Janz K, et al. L-type Calcium Channel Ca v 1.2 Is required for maintenance of auditory brainstem nuclei. *J Biol Chem*. 2015;290:23692-23710.
69. Korn MJ, Cramer KS. Distribution of glial-associated proteins in the developing chick auditory brainstem. *Dev Neurobiol*. 2008;68:1093-1106.
70. Cramer KS, Rubel EW. Glial Cell Contributions to Auditory Brainstem Development. *Front Neural Circuits*. 2016;10:83.
71. Yang Q, Feng B, Zhang K, et al. Excessive astrocyte-derived neurotrophin-3 contributes to the abnormal neuronal dendritic development in a mouse model of fragile X syndrome. *PLoS Genet*. 2012;8:e1003172.